JOURNAL OF AIRCRAFT
Vol. 35, No. 4, July–August 1998

Similarities Between Solid and Thin-Walled Composite Beams by Analytic Approach

Omri Rand*
Technion—Israel Institute of Technology, Technion City, Haifa 32000, Israel

This paper presents a study of the similarities between solid and thin-walled composite beams. The study is based on a set of closed-form solutions for simple solid and thin-walled composite-beam configurations. The prediction capability of these solutions is explored using available experimental data and by means of correlation with theoretical results provided by numerical codes. The study includes the basic lamination modes, covers all loading modes, and presents an important physical insight into the structural behavior and the coupling mechanisms. The findings clearly indicate important similarities in the structural behavior of solid and thin-walled beams. The results indicate that the proposed analytic solutions represent correctly the beam-like behavior of composite beams regardless of their specific cross-sectional geometry and lamination mode. In general, it is shown that by providing a clear insight and correct structural characteristics, the analytic solutions being examined may be used as a preliminary analysis tool for new designs.

Introduction

COMPOSITE structures provide numerous advantages and benefits over conventional aerospace materials. Among these advantages it is important to note their high specific strength, formability, and resistance to fatigue cracking and corrosion. Subsequently, composite beams are used as the primary structural components in many applications. In most of the cases, their high strength-to-weight ratio and improved fatigue characteristics are the main reasons for their selection during the design process.[1] However, in many aerospace structures, the potential of exploiting the structural couplings seems to be very attractive, and it is expected that these couplings may be used for improving the structure performance in many aspects beyond the static stiffness. Helicopter blades that are traditionally treated as beams are a relevant example for such use.[2,3] In this case, one may exploit favorable structural couplings to suppress vibration and augment stability margins.

Examination of the current structural models capable of dealing with composite beams shows that compared with isotropic beams, the analysis of composite beams is by far more complicated, and includes many more unknowns and degrees of freedom.

The present paper concentrates on the structural behavior of composite beams, to which a considerable amount of research work has been devoted during the last two decades. Therefore, the following will be devoted to these aspects. However, it is important to mention that the research of composite structures and the study of the adequacy of composites to a wide range of engineering applications has grown in many other directions such as failure mechanisms, delamination phenomena, and environmental conditions.[4–6]

A relatively large portion of the models for composite-beam analysis deals with thin laminated beams that may also be viewed as slender plates (plate-beam models).[7–11] These analyses demonstrate the importance of modeling the shear deformation (or the out-of-plane warping). This shear deformation has a crucial influence on the structural behavior and the associated couplings, and its correct description usually requires the utilization of numerical schemes. Shear deformation is also crucial for predicting stress singularities.[12–14]

The literature also contains detailed numerical analyses that are capable of providing relatively accurate predictions of the structural behavior of composite beams. Typically, such predictions must be based on a relatively large number of unknowns.[15–20] These types of modes are usually finite-element-based schemes and are capable of taking into account a detailed deformation field including both the in-plane and the out-of-plane warping effects and geometrical nonlinearities. Finite-difference-based models are reported in Refs. 21 and 22 for linear and nonlinear analysis of both thin-walled and solid-composite beams.

Very few experimental studies are reported in the literature. References 23–26 contain valuable experimental data that may be directly used for validating general theoretical models of composite beams. While Refs. 23 and 24 concentrate on the nonlinear behavior of laminated (solid) composite beams (plate-beam models), Ref. 25 deals with thin-walled box-beams, and Ref. 26 concentrates on the structural behavior of I-beams.

Unlike the well-known strength of materials solutions for isotropic beams, there are only limited fundamental closed-form exact analytic solutions for composite beams. Reference 27 presents an analytic approach for thin-walled beams that is based on a variational and asymptotical theory. However, Refs. 22 and 28 present a set of closed-form solutions for solid and thin-walled beams. Although these solutions are exact, they are restricted to certain geometries and lamination modes. Their advantage emerges from their potential to provide insight and clear identification of the major parameters that control the composite-beam behavior and the resulting structural couplings.

The present paper reviews the previously mentioned closed-form analytic solutions for solid and thin-walled composite beams, and by being compared with available experimental results and numerical models, this study enables the generalization of results, and the identification of similarities between the beam-like behaviors of different solid and thin-walled configurations.

Analytic Models for Solid and Thin-Walled Composite Beams

Deformation

Figure 1a presents a slender, straight, and untwisted composite beam of solid cross section, whereas Fig. 1b presents

Received Oct. 6, 1996; revision received Nov. 30, 1997; accepted for publication Jan. 9, 1998.

*Associate Professor, Faculty of Aerospace Engineering.

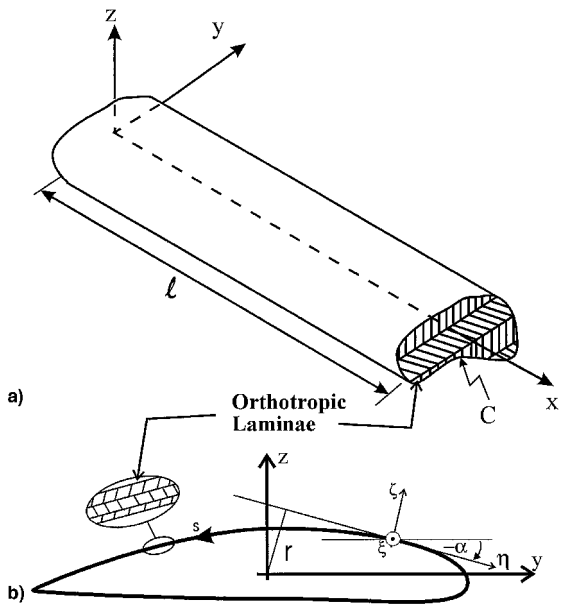

Fig. 1 a) Scheme of a straight, uniform, and untwisted composite beam of solid cross section and b) a thin-walled cross section.

the notation for a thin-walled cross section. The beam length l is stretched along the x axis, whereas the coordinates y and z define the cross-sectional planes. For a thin-walled cross section, it is convenient to define a local system of coordinates that is attached to the contour so that ξ is parallel to the x direction and η is tangent to the local contour (Fig. 1b). The angle α is measured between the y and η directions, and r is the normal distance to the tangent to the contour at the point under discussion. The beam is assumed to consist of orthotropic laminae that are parallel to the x–y plane in the case of a solid cross section, or parallel to the local ξ–η plane, i.e., parallel to the local wall direction, in the case of a thin-walled cross section.

Deformation is based on four cross-sectional displacements that are functions of x only, and one three-dimensional out-of-plane warping function. The cross-sectional displacements are the displacements $u(x)$, $v(x)$, and $w(x)$ in the x, y, and z directions, respectively, and the twist angle, $\phi(x)$, about the x direction. The three-dimensional warping function is denoted Ψ. For solid cross sections, Ψ is a function of x, y, and z. For thin-walled cross sections, the variation of Ψ through the wall thickness is neglected and, therefore, Ψ is a function of ξ (or x) and s, where s is a circumferential coordinate along the wall (Fig. 1b). In both cases Ψ should be a single-value continuous function that has a zero-average value over the cross-sectional area.

Strain Components

The following formulation is confined to the linear case in which no distinction between the deformed and the undeformed directions in required, and the preceding assumed deformation components may be directly used to construct the strain expressions. For this linear case, the nonvanishing strain components for a solid cross section are given by

$$\varepsilon_{xx} = u_{,x} - yv_{,xx} - zw_{,xx} + \Psi_{,x} \tag{1a}$$

$$\gamma_{xz} = y\phi_{,x} + \Psi_{,z} \tag{1b}$$

$$\gamma_{xy} = -z\phi_{,x} + \Psi_{,y} \tag{1c}$$

where ε_{xx} is the normal strain, and γ_{xz} and γ_{xy} are the shear strains. $(\,)_{,x}$ denotes differentiation with respect to x (or ξ). For a thin-walled cross section, the only nonzero linear strain components are the normal strain $\varepsilon_{\xi\xi}$ and the shear strain along the wall $\gamma_{\xi\eta}$, which are given by

$$\varepsilon_{\xi\xi} = u_{,x} - yv_{,xx} - zw_{,xx} + \Psi_{,x} \tag{2a}$$

$$\gamma_{\xi\eta} = -r\phi_{,x} - \Psi_{,s} \tag{2b}$$

Constitutive Relations

For a solid cross section, the constitutive relations are obtained by exploiting the beam slenderness and assuming $\sigma_{yy} = \sigma_{zz} = \tau_{yz} = 0$. This assumption has proven to be exact in the isotropic case, e.g., Ref. 29, and it may be shown analytically to be true in the case of homogeneous composite beam of solid cross section under pure bending moment as well. Consequently, a shown in the Appendix, it is possible to express the relations between stress components that act over the solid cross-sectional area and the preceding strain components by

$$\begin{pmatrix} \sigma_{xx} \\ \tau_{xz} \\ \tau_{xy} \end{pmatrix} = \begin{bmatrix} C_{11} & 0 & C_{16} \\ 0 & C_{55} & 0 \\ C_{16} & 0 & C_{66} \end{bmatrix} \begin{pmatrix} \varepsilon_{xx} \\ \gamma_{xz} \\ \gamma_{xy} \end{pmatrix} \tag{3}$$

The elastic moduli C_{ij} are functions of the material properties and the local ply angle relative to the x axis, e.g., Ref. 30. Note that the strains ε_{yy} and ε_{zz} are not zero [these strains may be determined based on the values of the strain components ε_{xx} and γ_{xy} as shown in Eq. (A5)] and, thus, Poisson's ratio effects are included in the previously presented formulation.

For a thin-walled cross section, the preceding material constitutive relations are applicable in the local ξ, η, and ζ system directions. By assuming $\sigma_{\eta\eta} = \sigma_{\zeta\zeta} = \tau_{\xi\zeta} = \tau_{\eta\zeta} = 0$, these relations may be reduced to

$$\begin{pmatrix} \sigma_{\xi\xi} \\ \tau_{\xi\eta} \end{pmatrix} = \begin{bmatrix} C_{11} & C_{16} \\ C_{16} & C_{66} \end{bmatrix} \begin{pmatrix} \varepsilon_{\xi\xi} \\ \gamma_{\xi\eta} \end{pmatrix} \tag{4}$$

For cases of nonuniform ply properties, a methodology for creating three-dimensional effective elastic constants might be helpful. Such efficient methodology is described in Ref. 31.

Equations of Equilibrium

Four integral equilibrium equations are derived for the four cross-sectional displacement components, and one differential (local) equation is derived for the warping function. The integral equations equate the cross-sectional resultants P (in the x direction), F_y (in the y direction), F_z (in the z direction), and the moment resultant M_x (in the x direction) that are obtained by the external loads to those obtained by stress integrations. For solid cross sections these equations become

$$(P, F_y, F_y, F_z, M_x) = \int\int_A (\sigma_{xx}, \tau_{xy}, \tau_{xz}, \tau_{xz}y - \tau_{xy}z)\, \mathrm{d}A \tag{5}$$

The differential equation of equilibrium for solid cross sections is the associated differential equilibrium equation in the x direction that is given by

$$\sigma_{xx,x} + \tau_{xy,y} + \tau_{xz,z} + B_x = 0 \tag{6}$$

where B_x is the body force in the x direction. Similarly, the corresponding integral equilibrium equations may be written for a thin-walled cross section as

$$(P, F_y, F_z, M_x) = \int_s\int_t (\sigma_{\xi\xi}, \tau_{\xi\eta}\cos\alpha, \tau_{\xi\eta}\sin\alpha, -r\tau_{\xi\eta})\, \mathrm{d}\zeta\, \mathrm{d}s \tag{7}$$

where, as shown, the integration is taken over the thickness and along the cross-sectional circumference to account for alll stresses over the cross-sectional area. The differential equilibrium equation takes the form

$$\sigma_{\xi\xi,\xi} + \tau_{\xi\eta,\eta} + B_\xi = 0 \tag{8}$$

Note that the preceding formulation consistently includes body forces in the x direction (B_x or B_ξ) and, therefore, may adequately be used to predict the effect of axial (centrifugal) loads on the behavior of composite rotating blades.

Boundary Conditions

There are eight boundary conditions at the beam root and tip. For a clamped beam, the geometrical boundary conditions at the beam root are

$$u = v = v_{,x} = w = w_{,x} = \phi = 0 \tag{9}$$

The natural boundary conditions at the beam tip are based on equating the external transverse tip moments, M_y^t and M_z^t, to those obtained by stress integrations over the tip cross-sectional area A^t. These conditions may be written as

$$(M_y^t, M_z^t) = \int\int_{A^t} (\sigma_{xx} z, -\sigma_{xx} y)\, dA^t \tag{10}$$

where in the case of a thin-walled cross-section, σ_{xx} should be replaced with $\sigma_{\xi\xi}$. For a solid cross section there is additional essential contour boundary condition that ensures no shear-stress flow through the contour, namely,

$$\tau_N = 0 \quad \text{on} \quad C \tag{11}$$

where τ_N is the shear stress normal to the contour C (Fig. 1a).

Analytic Solutions, Correlation, and Discussion

The analytic solutions presented in this paper were derived for simplified configurations that enable closed-form solutions and capture the main structural mechanisms (part of these solutions appear with more details in Ref. 22). For example, solid symmetric beams are represented by homogeneous cross sections where all laminae are identical and oriented at the same angle with respect to the x axis (which may be also viewed as single lamina cross sections). Because the elastic moduli are all constants in such cases, it is convenient to apply analytic techniques for their analysis. The geometry and the lamination modes for the thin-walled cross sections are described later.

The following discussion is first concentrated in symmetric beams and includes the influence of tensile forces P, torsional moments M_x, beamwise moments M_y, edgewise moments M_z, beamwise forces F_z, and edgewise forces F_y. Then, antisymmetric beams are discussed through the influence of P and M_x. Where available, the applicability of the proposed generalized solutions is demonstrated by correlation with experimental and numerical results.

Symmetric Beams

Tip Tensile Force

Solid cross section: When a homogeneous solid symmetric beam of arbitrary geometry is subjected to a tip tensile force, P^t, the preceding equilibrium equations [Eqs. (5)] and boundary conditions [Eqs. (9) and (11)] are fulfilled by setting $v_{,xx}$, $w_{,xx}$, and $\phi_{,x}$ to zero and

$$u_{,x} = \frac{P^t}{A}\frac{C_{66}}{C_{11}C_{66} - C_{16}^2} \tag{12a}$$

$$\Psi = -\frac{P^t}{A}\frac{C_{16}}{C_{11}C_{66} - C_{16}^2}\, y \tag{12b}$$

$$\gamma_{xy} = -\frac{P^t}{A}\frac{C_{16}}{C_{11}C_{66} - C_{16}^2} \tag{12c}$$

As indicated by Eq. (12a), the longitudinal strain variation is determined by the three elastic moduli C_{11}, C_{66}, and C_{16} (C_{55} does not participate). Thus, the approximation $u_{,x} = P^t/AC_{11}$ may induce significant discrepancies. For typical graphite/epoxy properties ($E_{11} = 130 \times 10^9$ N/m^2, $E_{22} = E_{33} = 12 \times 10^9$ N/m^2, $G_{12} = G_{13} = 6 \times 10^9$ N/m^2, $G_{23} = 4 \times 10^9$ N/m^2, $\nu_{12} = \nu_{13} = 0.3$, $\nu_{23} = 0.5$), an error of about 50% is obtained for a ply angle of 30 deg. Equation (12b) shows that in this case the warping is a linear function of y, and Eq. (12c) shows that the shear strain in the y direction is a negative constant.

A thin-walled cross section: To facilitate the discussion of a thin-walled symmetric beam, the cross section of arbitrary geometry shown in Fig. 2a will be studied. In this cross section, the part for which $0 \le s \le p/2$ (where p is the cross-sectional circumference) is assumed to be characterized by the elastic moduli C_{11}, C_{66}, and C_{16}, whereas the part for which $p/2 \le s \le p$ is characterized by C_{11}, C_{66}, and $-C_{16}$. A specific example for this case is the rectangular (box-beam) cross section shown in Fig. 2a, where the upper part of this cross section, i.e., for $z > 0$ or $0 \le s \le (a + b)$, is assumed to be characterized by the elastic moduli C_{11}, C_{66}, and C_{16}, whereas the lower part, i.e., for $z < 0$ or $(a + b) \le s \le 2(a + b)$, is characterized by C_{11}, C_{66}, and $-C_{16}$. Such a cross section may be obtained by lamination angles of opposite signs for the upper and lower parts (note that the lamination angles are relative to the local system of coordinates ξ, η, and ζ shown in Fig. 1b).

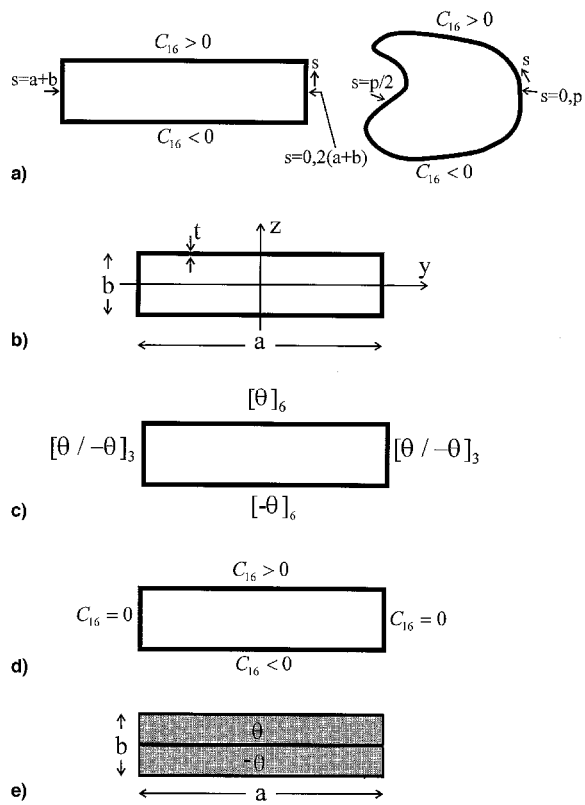

Fig. 2 Illustrative thin-walled and solid cross sections: a) elastic moduli distribution in an example symmetric lamination mode where $C_{16} > 0$ for $0 \le s \le p/2$ and $C_{16} < 0$ for $p/2 \le s \le p$, b) dimensions of a thin-walled box-beam, c) lamination angle distribution in an example symmetric lamination mode, d) distribution of C_{16} for the cross section presented in c), and e) an antisymmetric solid beam made of two laminae of opposite layup angles.

To derive an analytic solution for this case, it is convenient to start with the uncoupled case where $C_{16} = 0$ (while C_{11} and C_{66} are kept unchanged). In this case, it is clear that $v = w = \phi = \Psi = 0$ and $u_{,x} = P^t/C_{11}pt$. When a nonzero value of C_{16} is considered, additional strains $\Delta\varepsilon_{\xi\xi} = \Delta u_{,x}$ and $\Delta\gamma_{\xi\eta} = -\Psi_{,s}$ should appear to provide the same stress distribution (and, therefore, both equilibrium equations and boundary conditions will remain satisfied). To generate an exact closed-form analytic solution for this case, Ψ is assumed to be a linear function of the circumferential coordinate s (see Fig. 2a) given by

$$\Psi(s) = \alpha[s - (p/4)] \quad \text{for} \quad 0 \le s \le (p/2)$$
$$= \alpha(\tfrac{3}{4}p - s) \quad \text{for} \quad (p/2) \le s \le p \tag{13}$$

where α is a constant to be determined. Note that this distribution satisfies the requirements $\oint \Psi_{,s}\, ds = 0$ and $\oint \Psi\, ds = 0$. The requirement for zero additional stresses yields [see Eq. (4)]

$$\Delta\sigma_{\xi\xi} = C_{11}\Delta u_{,x} - C_{16}\alpha = 0 \tag{14a}$$

$$\Delta\tau_{\xi\eta} = C_{16}(u_{,x} + \Delta u_{,x}) - C_{66}\alpha = 0 \tag{14b}$$

It should be emphasized that because both the elastic modulus C_{16} and $\Psi_{,s}$ have opposite signs in the upper and lower parts of the cross section, Eqs. (14a) and (14b) hold for the entire beam. The solution of these equations yields the values of $\Delta u_{,x}$ and α in terms of the uncoupled axial strain $u_{,x}$. Using these values, the axial extension, the warping, and the shear strain may be written as

$$u_{,x} + \Delta u_{,x} = \frac{P^t}{pt}\frac{C_{66}}{C_{11}C_{66} - C_{16}^2} \tag{15a}$$

$$\Psi_{,s} = -\Delta\gamma_{\xi\eta} = \frac{P^t}{pt}\frac{C_{16}}{C_{11}C_{66} - C_{16}^2} \tag{15b}$$

The preceding closed-form solutions for symmetric solid and thin-walled composite beams reveal some interesting similarities. First, it should be noted that Eq. (12a) (that has been developed for a solid cross section of arbitrary geometry) holds for the thin-walled case as well (by replacing A with pt) and, therefore, the change in the axial stiffness shown by Eq. (12a) applies to both solid and thin-walled cross sections. Also, similar to the case of a solid cross section, the warping distribution over the upper and lower parts of the cross section (the upper and lower flanges in the case of a box-beam) is a linear function of s.

Further generalization of Eq. (12a) is based on replacing P^t with $P(x)$ and considering all other quantities in this equation as functions of x.

Tip Moments

General solution for solid cross section: It may be shown that the tip moments M_x^t, M_y^t, and M_z^t (in the x, y, and z directions, respectively), induce constant curvature components $w_{,xx}$, $v_{,xx}$, and twist $\phi_{,x}$ along the beam. To derive an exact solution for this case for a homogeneous solid cross section of arbitrary geometry, the uncoupled case is first examined. The uncoupled case is obtained by setting C_{16} to zero, and keeping the remaining moduli C_{11}, C_{66}, and C_{55} unchanged. In this uncoupled case, the torsional moment M_x^t is the only contributor to the warping. Here, it is convenient to adopt the closed-form analytic solution procedure of Ref. 32, that yields the torsional rigidity D (defined by $M_x^t/\phi_{,x}$) and the associated two-dimensional warping function $\varsigma(y, z)$.

The twist and the warping in the coupled case are assumed to be the following functions of D and $\varsigma(y, z)$:

$$\phi_{,x} = \frac{M_x^t}{D} - \frac{C_{16}}{2C_{66}}w_{,xx} \tag{16a}$$

$$\Psi = \frac{M_x^t}{D}\varsigma(y, z) + \frac{C_{16}}{2C_{66}}(w_{,xx}yz + v_{,xx}y^2 - 2u_{,x}y) + \text{const} \tag{16b}$$

where the constant is determined to ensure zero-average warping distribution over the cross section. Based on Eqs. (1a–1c) and (3), the strains and the stresses in this case are obtained. The resulting shear stresses satisfy the contour boundary condition [Eq. (11)], the differential equilibrium equation [Eq. (6)], and the integral equilibrium equations for $F_y = 0$, $F_z = 0$, and $M_x = 0$ [Eq. (5)]. Adequate integrations of the normal stress σ_{xx} is carried out to satisfy the integral equation for the axial resultant load, $P = 0$, [Eq. (5)] and the natural boundary conditions [Eq. (10)]. This step yields the following system of three equations:

$$\begin{pmatrix} u_{,x} \\ v_{,xx} \\ w_{,xx} \end{pmatrix} = \begin{bmatrix} A & -I_y & -I_z \\ I_y & -I_{yy} & -I_{yz} \\ I_z & -I_{yz} & -I_{zz} \end{bmatrix}^{-1} \times \begin{bmatrix} P^t - C_{16}(M_x^t/D)(I_\varsigma - I_z) \\ -M_z^t - C_{16}(M_x^t/D)(I_{\varsigma y} - I_{yz}) \\ M_y^t - C_{16}(M_x^t/D)(I_{\varsigma z} - I_{zz}) \end{bmatrix} \frac{C_{66}}{C_{11}C_{66} - C_{16}^2} \tag{17}$$

where

$$(A, I_y, I_z, I_{yz}, I_{yy}, I_{zz}, I_\varsigma, I_{\varsigma y}, I_{\varsigma z}) = \int\int_A \left(1, y, z, yz, y^2, z^2, \frac{\partial\varsigma}{\partial y}, y\frac{\partial\varsigma}{\partial y}, z\frac{\partial\varsigma}{\partial y}\right) dA \tag{18}$$

To simplify the preceding general expression, the origin of the system of coordinates is assumed to be located at the cross-sectional area center, yielding $I_y = I_z = 0$. In addition, it may be shown that $I_\varsigma = 0$, and that $I_{yz} = I_{\varsigma y} = 0$ for a cross section that exhibits symmetry about the z axis. For such cases a separate discussion will be devoted to the torsional and the transverse tip moments.

Tip torsional moment (M_x^t): In this case, Eqs. (16a) and (17) show that $u_{,x}$ and $v_{,xx}$ vanish and:

$$w_{,xx} = -r_z\frac{M_x^t}{D}\frac{C_{16}C_{66}}{C_{11}C_{66} - C_{16}^2} \tag{19a}$$

$$\phi_{,x} = \frac{M_x^t}{D}\left[1 + \frac{C_{16}^2}{2(C_{11}C_{66} - C_{16}^2)}r_z\right] \tag{19b}$$

where r_z is a nondimensional parameter given by

$$r_z = 1 - (I_{\varsigma z}/I_{zz}) \tag{20}$$

Equations (19a) and (19b) show that the effect of the coupling moduli C_{16} is controlled by r_z. Following the solution procedure of Ref. 32 for determining $\varsigma(y, z)$ and Eqs. (18) and (20), r_z may be evaluated. Alternatively, it is possible to show that r_z may be expressed as

$$r_z = \frac{D}{2I_{zz}C_{66}} \tag{21}$$

Expressions for r_z for rectangular and elliptic cross sections are presented in Ref. 28. It turns out that r_z may be expressed as a function of the nondimensional parameter q that combines geometry and elastic characteristics given by

$$q = (a/b)\sqrt{(C_{55}/C_{66})} \tag{22}$$

Generally, r_z is a monotonic increasing function of q and is bounded by $0 \le r_z \le 2$. For a thin rectangular cross section (plate-beam model), high values of q are obtained, yielding r_z

$\cong 2$. For a square cross section that is made of transversely isotropic material (where $C_{55} = C_{66}$ and $q = 1$), $r_z \cong 0.84$ is obtained.

Generalization to the case of thin-walled cross section: Equations (19a) and (19b) show that a tip torsional moment induces a constant bending curvative and a constant twist, and their ratio is given by

$$\frac{w_{,xx}}{\phi_{,x}} = -\frac{r_z C_{16} C_{66}}{C_{11}C_{66} + C_{16}^2[(r_z/2) - 1]} \tag{23}$$

To study the applicability of Eq. (23) to thin-walled symmetric cross sections, the experimental and calculated results of Ref. 25 were utilized. As reported in Ref. 25, thin-walled symmetric beams made of graphite/epoxy laminae ($E_{11} = 141 \times 10^9$ N/m^2, $E_{22} = 9.78 \times 10^9$ N/m^2, $G_{12} = 6.13 \times 10^9$ N/m^2, $\nu_{12} = 0.42$) were constructed as box-beams having $[\theta]_6$ and $[-\theta]_6$ at the top and bottom flanges, respectively, and $[\theta/-\theta]_3$ at the right and left webs (Fig. 2c) (the local system of coordinates ξ, η, and ζ is shown in Fig. 1b). This lamination mode results in a symmetric beam where the elastic modulus C_{16} is zero over the webs and has opposite signs over the flanges as described in Fig. 2d. The test results clearly indicate that $\phi(x)$ and $w_{,x}(x)$ are linear functions and, therefore, $w_{,xx}$ and $\phi_{,x}$ are constants for each test case. The predicted values of $w_{,xx}/\phi_{,x}$ obtained by Eq. (23) for solid cross sections are presented in 3a as a function of the right-hand sides (RHSs) of Eq. (23), and in Fig. 3b as a function of the lamination angle. In both cases the test and calculated results presented in Ref. 25 are also shown. For thin-walled cross sections, r_z is evaluated by Eq. (21), which yields

$$r_z = 2A_m^2 \Big/ I_{zz} \oint \frac{ds}{t} \tag{24}$$

where A_m is the area enclosed by the median line.

Figure 3 shows that although it was developed for solid cross sections, Eq. (23) is capable of predicting the elastic coupling in thin-walled cross sections as well (one should also keep in mind that there is a wide range of configurations that may be characterized as symmetric beams, and small variations in the predicted values are expected). Consequently, it may be concluded that the closed-form solution for the symmetric solid cross section presented in the preceding text correctly describes the twist–bending coupling mechanism induced in symmetric beams by torsional moment. In particular, it has been shown that the quantity on the RHS of Eq. (23) is the major factor in determining the present coupling mechanism. In addition, it appears that for symmetric beams, the value of $w_{,xx}/\phi_{,x}$ reaches a maximum of about 0.6 around a lamination angle of 40 deg.

Further generalization of Eqs. (19a) and (19b) is based on replacing M_x^t with $M_x(x)$ and considering all other quantities in these equations as functions of x.

Tip beamwise (M_y^t) and chordwise (M_z^t) moments: The curvature components and the twist caused by a transverse tip beamwise and chordwise moments are obtained from Eqs. (16a) and (17) as $u_{,x} = 0$ and

$$v_{,xx} = \frac{M_z^t}{I_{yy}} \frac{C_{66}}{C_{11}C_{66} - C_{16}^2} \tag{25a}$$

$$w_{,xx} = -\frac{M_y^t}{I_{zz}} \frac{C_{66}}{C_{11}C_{66} - C_{16}^2} \tag{25b}$$

$$\phi_{,x} = \frac{M_y^t}{2I_{zz}} \frac{C_{16}}{C_{11}C_{66} - C_{16}^2} \tag{25c}$$

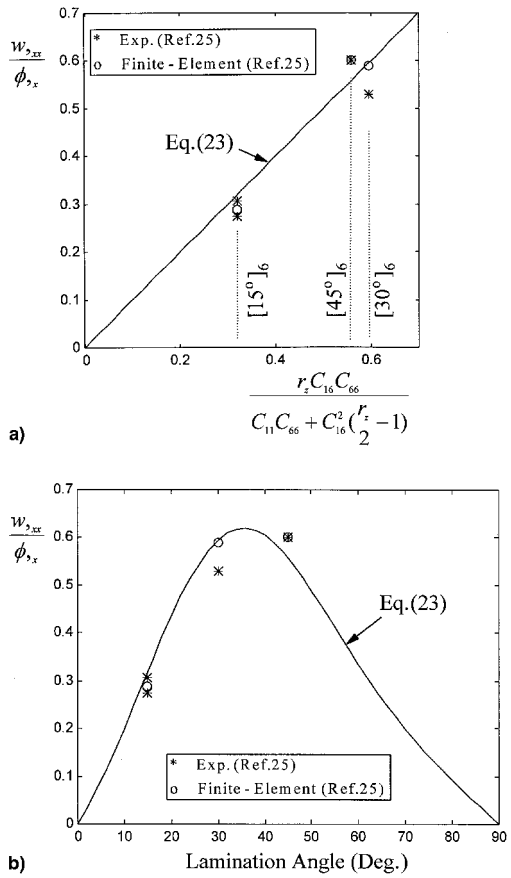

Fig. 3 Predicted values of $w_{,xx}/\phi_{,x}$ obtained by Eq. (23) for solid cross sections compared with test and calculated results presented in Ref. 25. As functions of the a) RHS of Eq. (23) and b) the lamination angle.

As shown, the twist–bending coupling caused by M_y^t is expressed by

$$\phi_{,x} = -\frac{C_{16}}{2C_{66}} w_{,xx} \tag{26}$$

which relates the twist and the beamwise bending curvature. Note that the same relation may be obtained by Eqs. (19a) and (19b) between the additional twist because of C_{16} and the bending curvature in the case of a tip torsional moment. Because Eqs. (25a–25c) indicate that the effects of beamwise and chordwise bending moments are functions of the elastic moduli C_{11}, C_{66}, and C_{16} only, i.e., C_{55} has no influence in these cases, by expressing the moments of inertia (I_{yy}, I_{zz}) correctly, Eqs. (25a–25c) may be directly applied to thin-walled cross sections as well.

Further generalization of Eqs. (25a–25c) is based on replacing M_y^t and M_z^t with $M_y(x)$ and $M_z(x)$, respectively, and considering all other quantities in these equations as functions of x.

Tip Beamwise Force

Solid cross section: The solution for a rectangular cross section (bounded by $y = \pm a/2$ and $z = \pm b/2$) undergoing a tip beamwise force (F_z^t) is initiated by assuming $u = v = 0$, and a warping function that is a sum of isotropic warping function and the warping obtained earlier for M_y^t, namely,

$$\Psi = -\frac{6F_z^t}{ab^3C_{55}}\left[\frac{z^3}{3} - \left(\frac{b}{2}\right)^2 z\right] - \phi_{,x} yz \tag{27}$$

Equations (1a–c) and (3) show that by neglecting the $\Psi_{,x}$ term, the resulting stresses are given by

$$\sigma_{xx} = -z(C_{11}w_{,xx} + 2C_{16}\phi_{,x}) \tag{28a}$$

$$\tau_{xz} = -\frac{6F_z^t}{ab^3}\left[z^2 - \left(\frac{b}{2}\right)^2\right] \tag{28b}$$

$$\tau_{xy} = -z(C_{16}w_{,xx} + 2C_{66}\phi_{,x}) \tag{28c}$$

As shown, τ_{xz} satisfies the boundary condition at $z = \pm b/2$ [see Eq. (11)]. However, because τ_{xy} is not a function of y, one should require $\tau_{xy} = 0$. This yields again the twist–bending curvature relation of Eq. (26). In addition, the differential equilibrium equation [Eq. (6)] shows that

$$w_{,xxx} = -\frac{12F_z^t}{ab^3}\frac{C_{66}}{C_{11}C_{66} - C_{16}^2} \tag{29}$$

The natural boundary conditions at the beam tip [Eq. (10)] show that $w_{,xx}(l) = 0$. Carrying out the longitudinal integrations, w and ϕ for a clamped beam become

$$w = \frac{2F_z^t}{ab^3}\frac{C_{66}}{C_{11}C_{66} - C_{16}^2}x^2(3l - x) \tag{30a}$$

$$\phi = -\frac{3F_z^t}{ab^3}\frac{C_{16}}{C_{11}C_{66} - C_{16}^2}x(2l - x) \tag{30b}$$

As already indicated, Eq. (26) turns to represent the twist–bending coupling mechanism. It has been shown in previous sections that for general solid cross sections, Eq. (26) appears to be valid for predicting the ratio of the additional twist to the bending curvature as a result of a tip torsional moment (M_x^t), and the ratio of the twist to the bending curvature as a result of a tip beamwise moment (M_y^t). The solution for a rectangular cross section presented earlier shows that Eq. (26) may also be used for determining the twist caused by a tip beamwise force.

Partial validation of the prediction capability of Eqs. (30a) and (30b) may be obtained by their correlation with the experimental results reported in Ref. 23 for a thin ($a/b = 20.4$) laminated beam made of graphite/epoxy ($E_{11} = 142 \times 10^9$ N/m^2, $E_{22} = 9.8 \times 10^9$ N/m^2, $G_{12} = 6 \times 10^9$ N/m^2, $\nu_{12} = 0.3$). Although these experiments were aimed toward the nonlinear behavior, Eq. (30a) may be utilized to predict the linear (small deformation) beamwise displacement (twist angle values are not reported in Ref. 23). The elastic moduli used in these predictions were obtained by smearing the actual moduli over the cross-sectional area. Figure 4 presents the beamwise displacements at 91% span location as functions of the tip beamwise load. The reasonable correlation presented in Fig. 4 demonstrates the capability of Eq. (30a) that has been developed for homogeneous cross sections to supply analytic prediction and an insight for a broader range of configurations.

Although Eqs. (30a) and (30b) were derived for a rectangular cross section, it is expected that they may serve as an approximate solution for other cross-sectional geometries including thin-walled cross sections by replacing ab^3 with $12I_{zz}$. To demonstate this capability, the tip beamwise displacement and the tip twist angle of a thin-walled symmetric box-beam (with elastic moduli distribution shown in Fig. 2e) were determined by the numerical scheme described in Ref. 21, and correlated with the prediction provided by Eqs. (30a) and (30b) (Fig. 5). For that purpose, Eqs. (30a) and (30b) were written as

$$w_t\frac{3C_{11}I_{zz}}{F_z^t l^3} = \frac{\tilde{C}_{66}}{\tilde{C}_{66} - \tilde{C}_{16}^2} \tag{31a}$$

$$\phi_t\frac{4C_{11}I_{zz}}{F_z^t l^2} = -\frac{\tilde{C}_{16}}{\tilde{C}_{66} - \tilde{C}_{16}^2} \tag{31b}$$

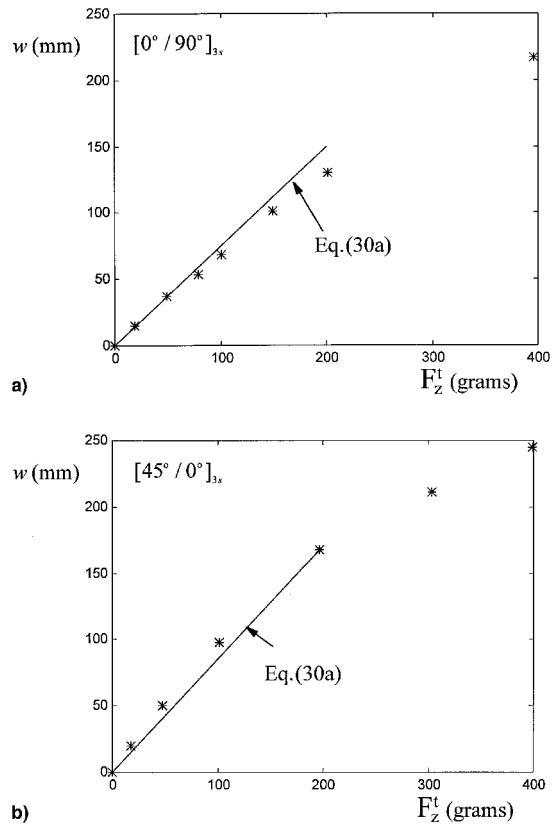

Fig. 4 Predicted values of the beamwise displacements as obtained by Eq. (30a) for thin laminated beams (plate-beam) as functions of the tip beamwise load, compared with test results presented in Ref. 23 (the displacements are measured at 91% span location).

where $\tilde{C}_{ij} = C_{ij}/C_{11}$. The good correlation presented by Fig. 5 leads to the conclusion that Eqs. (31a) and (31b) [or Eqs. (30a) and (30b)] do provide general expressions that describe the behavior of both solid and thin-walled symmetric beams. Although minor changes are possible because of the wide range of symmetric beam configurations, e.g., the different slopes in Fig. 5a, it appears that the RHS of Eqs. (31a) and (31b) are the major parameters that control the structural behavior in this case. The next section provides additional discussion of this point, and supplies analytic insight into the twist–bending coupling mechanism for a thin-walled analysis point of view.

Further generalization of Eqs. (30a) and (30b) is based on replacing F_z^t with $F_z(x)$, and considering all other quantities in these equations as functions of x. Numerical study has shown that the preceding prediction provides excellent correlation with numerical results even for cases where the distribution of the loads (or the beam characteristics) is described as a third-order polynomial function of x.

A thin-walled cross section: To derive the expressions for the elastic couplings in thin-walled beams caused by a tip beamwise load, the single-cell box-beam of constant wall thickness shown in Fig. 2b will be considered while the elastic moduli are assumed to be constants across the wall thickness. The shear stress in this case is given by [see Eqs. (2a), (2b), and (4)]

$$\tau_{\xi\eta} = C_{16}(-zw_{,xx} + \underline{\Psi_{,x}}) + C_{66}(-r\phi_{,x} - \Psi_{,s}) \tag{32}$$

where the underlined term will be neglected. Symmetry arguments show that $\oint \tau_{\xi\eta}\, ds = 0$, whereas displacement com-

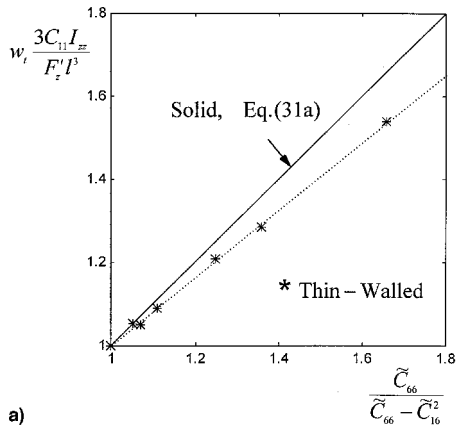

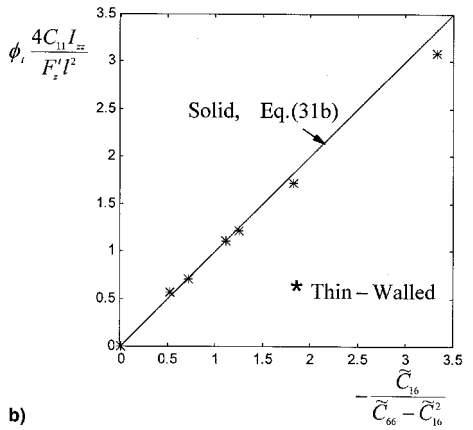

Fig. 5 Comparison between the tip deformation as predicted by the closed-form solution for solid beams [Eqs. (31a) and (31b)], and numerical results for a thin-walled configuration: a) tip beamwise displacement and b) tip twist angle.

patibility requires $\oint \Psi_{,s}\, ds = 0$. Consequently, Eq. (32) shows that

$$\frac{\phi_{,x}}{w_{,xx}} = \frac{\oint zC_{16}\, ds}{\oint rC_{66}\, ds} \tag{33}$$

Application of the preceding equation to two, slightly different thin-walled lamination modes will be discussed in what follows. First, the configuration shown in Fig. 2c and 2d is considered. Clearly, the lamination mode shown in Fig. 2c results in constant values of the elastic moduli C_{11} and C_{66}, a positive value of C_{16} over the upper flange, a negative value of C_{16} over the lower flange, and a zero value of C_{16} over the vertical webs as shown in Fig. 2d. For this case, it is easy to show that $\oint C_{66}r\, ds = 2abC_{66}$, $\oint zC_{16}\, ds = abC_{16}$. Substitution of these values in Eq. (33) again yields the twist–bending mechanism described by Eq. (26). However, for the configuration shown in Fig. 2b, where $C_{16} > 0$ for $z > 0$ and $C_{16} < 0$ for $z < 0$ (while C_{11} and C_{66} are still constants), the coupling magnitude described by Eq. (33) becomes

$$\frac{\phi_{,x}}{w_{,xx}} = -\frac{C_{16}}{2C_{66}}\left(1 + \frac{b}{2a}\right) \tag{34}$$

Figure 6 presents the ratio $\phi_{,x}/w_{,xx}$ for the configuration of Figs. 2c and 2d, which, as mentioned earlier, is given by Eq. (26). The values predicted by Eq. (26) are represented by the

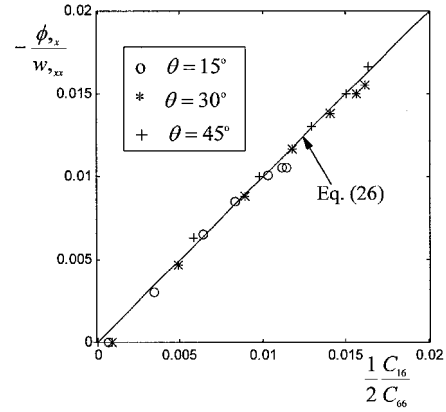

Fig. 6 Ratio $\phi_{,x}/w_{,xx}$ for the configuration of Figs. 2c and 2d. The values predicted by Eq. (26) are represented by the solid line. The symbols represent the test results for different spanwise locations reported in Ref. 25.

straight line, while the symbols represent the test results reported in Ref. 25. The excellent correlation supports the preceding findings regarding the coupling magnitude (note that the symbols in Fig. 6 are for different spanwise locations and for different lamination angles). It may be concluded that Eq. (26) represents the coupling mechanism in both solid and thin-walled symmetric beams; whereas, according to Eq. (33), slight differences in the lamination mode may induce differences similar to those shown by Eq. (34) for the configuration of Fig. 2b.

Tip Edgewise Force

In this case, an exact analytic solution for a rectangular cross section (bounded by $y = \pm a/2$ and $z = \pm b/2$) may be derived by assuming $w = \phi = 0$, and warping of the following shape:

$$\Psi = -\frac{6F_y^t}{a^3bC_{66}}\left[\frac{y^3}{3} - \left(\frac{a}{2}\right)^2 y\right] + \alpha y^3 + \beta(x - l)\left(y^2 - \frac{a^2}{12}\right) + \gamma y \tag{35}$$

where

$$\alpha = -\frac{C_{16}}{3C_{66}}\beta \tag{36a}$$

$$\beta = \frac{C_{16}}{2C_{66}}\frac{v_{,xx}}{x - l} \tag{36b}$$

$$\gamma = \frac{C_{16}}{C_{66}}\left(\frac{a^2\beta}{12} - u_{,x}\right) \tag{36c}$$

As will be shown, $v_{,xx}$ is proportional to $(x - l)$, and $u_{,x}$ is a constant. Therefore, α, β, and γ are all constants. Accordingly, Ψ is a function of both x and y. Using Eqs. (1a–1c) and (3) it is possible to express the stress components for this case as

$$\sigma_{xx} = \frac{C_{11}C_{66} - C_{16}^2}{C_{66}}\left[u_{,x} - yv_{,xx} + \beta\left(y^2 - \frac{a^2}{12}\right)\right] - \frac{6F_y^tC_{16}}{a^3bC_{66}}\left[y^2 - \left(\frac{a}{2}\right)^2\right] \tag{37a}$$

$$\tau_{xz} = 0 \tag{37b}$$

$$\tau_{xy} = -\frac{6F_y^t}{a^3b}\left[y^2 - \left(\frac{a}{2}\right)^2\right] \tag{37c}$$

Eqs. (37b) and (37c) show that the cross-sectional boundary

conditions are satisfied. The differential equilibrium equation [Eq. (6)] yields

$$v_{,xxx} = -\frac{12F_y^t}{a^3 b}\frac{C_{66}}{C_{11}C_{66} - C_{16}^2} \tag{38}$$

while the natural boundary conditions at the beam tip [Eq. (10)] show that

$$u_{,x} = -\frac{F_y^t}{ab}\frac{C_{16}}{C_{11}C_{66} - C_{16}^2} \tag{39}$$

Proper integrations for a clamped beam yields

$$v = \frac{2F_y^t}{a^3 b}\frac{C_{66}}{C_{11}C_{66} - C_{16}^2}x^2(3l - x) \tag{40a}$$

$$u = -\frac{F_y^t}{ab}\frac{C_{16}}{C_{11}C_{66} - C_{16}^2}x \tag{40b}$$

Similar to the case of beamwise and edgewise moments [see Eqs. (25a) and (25b)], C_{55} does not appear in the preceding formulation. Therefore, these expressions may be directly applied to beams of other cross-sectional geometries, including thin-walled cross sections. For that purpose, Eqs. (38) and (39) may be generalized by replacing $a^3 b$ with $12I_{yy}$, and ab by A. Accordingly, the present extension chordwise bending elastic coupling will be determined by

$$\frac{u_{,x}}{v_{,xxx}} = \frac{I_{yy}}{A}\frac{C_{16}}{C_{66}} \tag{41}$$

Further generalization is based on replacing F_y^t with $F_y(x)$ in Eq. (38), and considering all other quantities in this equation as functions of x.

Antisymmetric Beams

Analytic modeling of solid antisymmetric beams is relatively complicated because of the need to model cross sections of nonhomogeneous elastic moduli. However, when thin-walled cross sections are considered, a cross section with constant elastic moduli creates an antisymmetric lamination mode (again, it should be noted that the lamination angles are relative to the local system of coordinates ξ, η, and ζ shown in Fig. 1b). Therefore, the analytic insight into the coupling mechanisms in antisymmetric beams has been derived for a thin-walled cross section.

Tip Torsional Moment and a Tip Axial Force

Thin-walled cross section: The following modeling of an antisymmetric thin-walled beam is derived for a single-cell cross section of arbitrary geometry, constant wall thickness, and constant elastic moduli. When a beam of such cross section is subjected to a tip torsional moment (M_x^t) and a tip axial force (P^t), an exact analytic solution may be generated by assuming $v = w = 0$ and constant strains $\varepsilon_{\xi\xi}$ and $\gamma_{\xi\eta}$ over each cross section and along the beam. Consequently, $\sigma_{\xi\xi}$ and $\tau_{\xi\eta}$ are also constants, and Ψ is a function of s only (see Fig. 1). Consequently, Eq. (7) shows that

$$P^t = pt\sigma_{\xi\xi} \tag{42a}$$

$$M_x^t = -2A_m t\tau_{\xi\eta} \tag{42b}$$

where p is the cross-sectional circumference and A_m is the area enclosed by the median line. Because $\sigma_{\xi\xi}$ and $\tau_{\xi\eta}$ are constants, the differential equilibrium equation [Eq. (8)] is satisfied. Substitution of Eqs. (2a), (2b), and (4) into Eqs. (42a) and (42b) yields two equations for the unknowns $u_{,x}$ and $\phi_{,x}$. Solving these equations yields

$$\begin{pmatrix} u_{,x} \\ \phi_{,x} \end{pmatrix} = \frac{1}{t}\frac{1}{C_{11}C_{66} - C_{16}^2}\begin{bmatrix} C_{66}/p & C_{16}/2A_m \\ C_{16}/2A_m & C_{11}p/4A_m^2 \end{bmatrix}\begin{pmatrix} P^t \\ M_x^t \end{pmatrix} \tag{43}$$

The quality of the prediction provided by Eq. (43) for thin-walled beams may be assessed by the test results presented in Ref. 25. In these experiments, rectangular box beams made of uniformly distributed (in the circumferential direction) elastic moduli were tested. Three lamination modes were reported: $[15]_6$, $[0/30]_3$, and $[0/45]_3$. Equation (43) shows that for a tip torsional moment, equal values of $(\phi_{,x}/M_x^t)(4A_m^2 t/p)C_{11}$, and $C_{11}^2/(C_{11}C_{66} - C_{16}^2)$ are obtained. Figure 7a presents these quantities over its vertical and horizontal axes. The test results of Ref. 25 are also presented. Note that for the $[0/30]_3$ and $[0/45]_3$ lamination modes, the elastic moduli of the test results were smeared over the wall thickness. As shown, Eq. (43) predicts well the torsional rigidity in coupled thin-walled antisymmetric beams.

Similarly, Eq. (43) shows that for a tip axial force, equal values of $(\phi_{,x}/P^t)(2A_m t)C_{16}$ and $C_{16}^2/(C_{11}C_{66} - C_{16}^2)$ are obtained. Figure 7b presents these quantities and their correlation with the test results of Ref. 25. Again, reasonable correlation is observed and it may be concluded that Eq. (43) well represents also the extension–twist coupling in thin-walled antisymmetric beams.

Solid cross section: The generalization of the behavior of thin-walled antisymmetric beams under torsional moment and axial loads to the case of solid beams is based on the solution

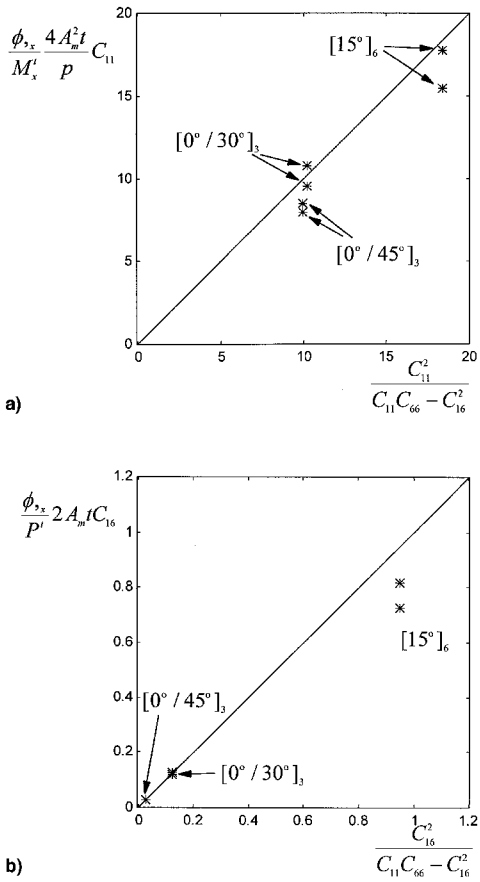

Fig. 7 Predicted values of the twist as obtained by Eq. (43) for a thin-walled antisymmetric beam compared with test results for different spanwise locations reported in Ref. 25. The twist caused by a) tip torsional moment and b) tip tensile force.

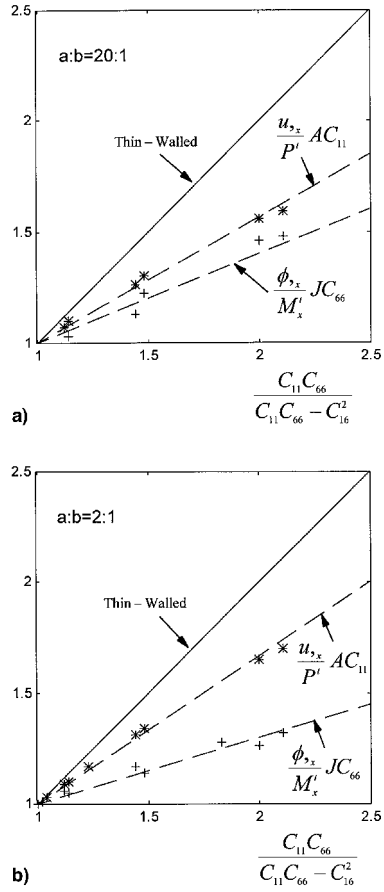

Fig. 8 Demonstration of the capability of Eq. (44) to predict the axial stiffness and the torsional rigidity for antisymmetric solid cross sections. The predicted results for a thin-walled cross section are represented by the solid line. The numerical results that were obtained for the configuration shown in Fig. 2e are represented by the symbols. The results for *a/b* = a) 20 and b) 2.

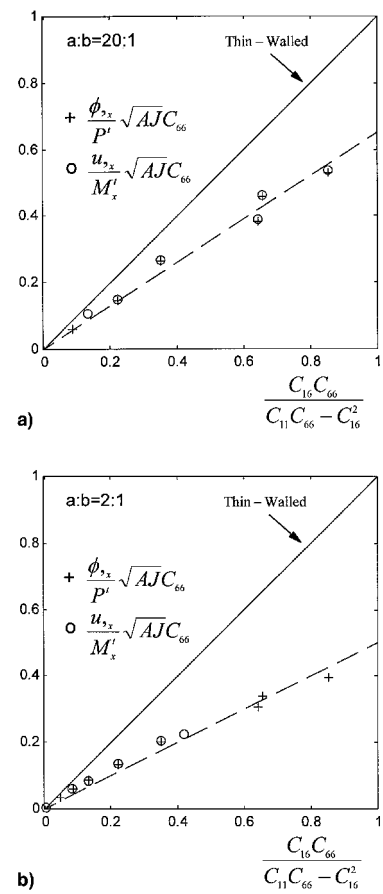

Fig. 9 Demonstration of the capability of Eq. (44) to predict the elastic couplings for antisymmetric solid cross sections. The predicted results for a thin-walled cross section are represented by the solid line. The numerical results that were obtained for the configuration shown in Fig. 2e are represented by the symbols. The results for *a/b* = a) 20 and b) 2.

presented by Eq. (43). Recalling that for the thin-walled case the torsional rigidity may be expressed as $J = 4A_m^2 t/p$, and the cross-sectional area as $A = pt$, Eq. (43) may be written as

$$\begin{pmatrix} u_{,x} \\ \phi_{,x} \end{pmatrix} = \frac{1}{C_{11}C_{66} - C_{16}^2} \begin{bmatrix} (C_{66}/A) & (C_{16}/\sqrt{AJ}) \\ (C_{16}/\sqrt{AJ}) & (C_{11}/J) \end{bmatrix} \begin{pmatrix} P^t \\ M_x^t \end{pmatrix} \tag{44}$$

Validation of the coupling mechanism generalization presented by Eq. (44) was carried out by the rectangular antisymmetric solid beam presented in Fig. 2e. As shown, the cross section consists of two laminae of opposite layup angles. The calculations were carried out using the numerical scheme reported in Ref. 22.

The twist caused by a tip torsional moment and the axial extension caused by a tip axial force [the diagonal terms in Eq. (44)] may be nondimensionalized as $(\phi_{,x} JC_{66}/M_x^t)$ and $(u_{,x} AC_{11}/P^t)$, respectively. Equation (44) shows that these quantities are both equal to the ratio $(C_{11}C_{66})/(C_{11}C_{66} - C_{16}^2)$. This identity is presented in Figs. 8a and 8b by the solid lines. The symbols are numerical results obtained for the preceding antisymmetric solid beam. Figures 8a and 8b demonstrate that the ratio $(C_{11}C_{66})/(C_{11}C_{66} - C_{16}^2)$ is indeed the most important quantity in the determination of the extensional stiffness and the torsional rigidity of both thin-walled and antisymmetric beams. The results presented in Figs. 8a and 8b may be formulated as

$$\frac{\phi_{,x}}{M_x^t} JC_{66} = 1 + \gamma_\phi \left(\frac{C_{11}C_{66}}{C_{11}C_{66} - C_{16}^2} - 1 \right) \tag{45a}$$

$$\frac{u_{,x}}{P^t} AC_{11} = 1 + \gamma_u \left(\frac{C_{11}C_{66}}{C_{11}C_{66} - C_{16}^2} - 1 \right) \tag{45b}$$

where for thin-walled cross sections $\gamma_\phi = \gamma_u = 1$, and for the solid cross section under discussion, $\gamma_\phi \cong 0.40$, $\gamma_u \cong 0.57$ for $a/b = 20$, and $\gamma_\phi \cong 0.30$, $\gamma_u \cong 0.67$ for $a/b = 2$. Clearly, for $C_{16} = 0$, the quantities on the RHS of Eqs. (45a) and (45b) become units.

The coupling terms that represent the axial extension because of a tip torsional moment and the twist because of a tip axial force, may be nondimensionalized as $u_{,x}\sqrt{AJ}/M_x^t$ and $\phi_{,x}\sqrt{AJ}/P^t$, respectively. Equation (44) shows that these off-diagonal terms are both equal to $C_{16}/(C_{11}C_{66} - C_{16}^2)$. This relation is presented in Figs. 9a and 9b (where for the sake of convenience all values were multiplied by C_{66}). As expected, the coupling magnitudes are identical; however, the coupling magnitude in the case of $a/b = 20$ is larger than that obtained for $a/b = 2$. The results presented in Figs 9a and 9b may be generalized as

$$\frac{\phi_{,x}}{P^t} = \frac{u_{,x}}{M_x^t} = \gamma_{\phi u} \frac{1}{\sqrt{AJ}} \frac{C_{16}}{C_{11}C_{66} - C_{16}^2} \tag{46}$$

where for thin-walled cross sections $\gamma_{\phi u} = 1$, and for the solid cross section under discussion, $\gamma_{\phi u} \cong 0.65$ for $a/b = 20$, and $\gamma_{\phi u} \cong 0.50$ for $a/b = 2$. It is therefore evident that the amount of twist per unit axial force and the amount of axial extension per unit torsional moment in thick solid cross sections are about half of their magnitudes in thin-walled cross sections.

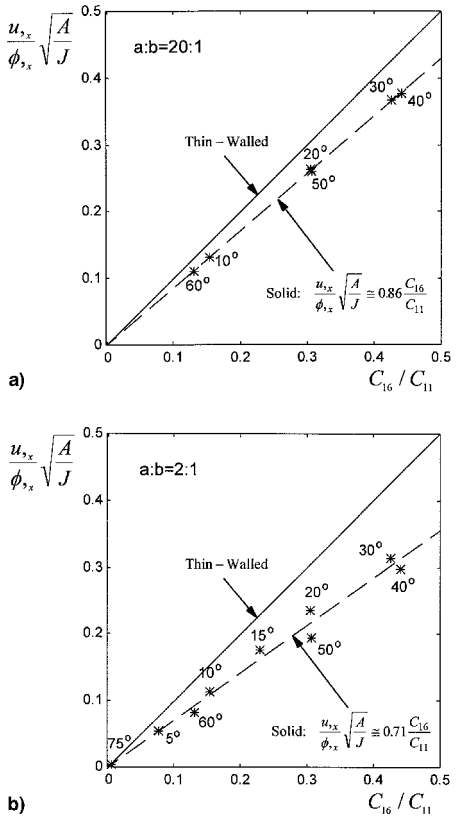

Fig. 10 Demonstration of the capability of Eq. (44) to predict the amount of axial extension per unit twist in the presence of a tip torsional moment for antisymmetric solid cross sections. The predicted results are represented by the solid line. The numerical results that were obtained for the configuration shown in Fig. 2e are represented by the symbols. The results for *a/b* = a) 20 and b) 2.

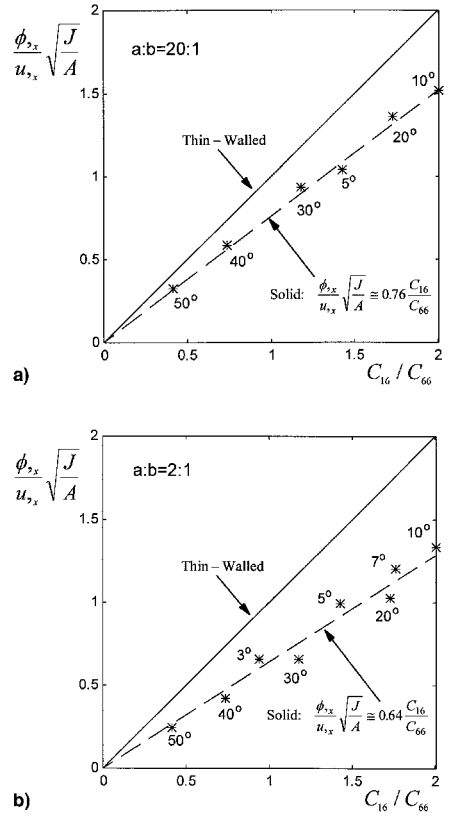

Fig. 11 Demonstration of the capability of Eq. (44) to predict the amount of twist per unit axial extension in the presence of a tip axial force for antisymmetric solid cross sections. The predicted results are represented by the solid line. The numerical results that were obtained for the configuration shown in Fig. 2e are represented by the symbols. The results for *a/b* = a) 20 and b) 2.

In addition, it is interesting to examine the overall behavior of the extension–twist elastic coupling terms for thin-walled and solid cross sections. Equation (44) shows that for a tip torsional moment, the extension–twist elastic coupling is given by

$$\frac{u_{,x}}{\phi_{,x}}\sqrt{\frac{A}{J}} = \frac{C_{16}}{C_{11}} \tag{47}$$

The solid line in Figs. 10a and 10b represents the above Eq. (47). The symbols are numerical results obtained for the antisymmetric solid beam under discussion. The lamination angles (θ, see Fig. 2e) are also indicated. As shown in Fig. 10a, in the case of $a/b = 20$ it is evident that like the case of thin-walled beams, the ratio C_{16}/C_{11} is the most important parameter that controls the extension–torsion coupling. For a thicker cross section of $a/b = 2$, Fig. 10b shows that the calculated results are more scattered; however, it is still evident that the ratio C_{16}/C_{11} is the major parameter in the determination of the elastic couplings as well. For a tip axial force, Eq. (44) shows that

$$\frac{\phi_{,x}}{u_{,x}}\sqrt{\frac{J}{A}} = \frac{C_{16}}{C_{66}} \tag{48}$$

Figure 11a presents the preceding coupling by the solid line, and the calculated results for a solid beam of $a/b = 20$ are represented by the symbols along with the corresponding lamination angles. Figure 11b presents the values for a thicker cross section, where $a/b = 2$. Consequently, it is clear that the ratio C_{16}/C_{66} controls the extension–torsion coupling in this case.

It should be noted that by definition, the origin in Figs. 8–11 includes the values for θ = 0 and 90 deg.

Based on the results presented in Figs. 10 and 11 it is possible to conclude that the couplings in antisymmetric beams are linearly correlated with the elastic moduli ratios C_{16}/C_{11} and C_{16}/C_{66}, and with the geometrical quantity $\sqrt{J/A}$.

Further generalization of Eq. (44) is based on replacing P' and M'_x with P and M_x, respectively, to reflect the possibility to determine $u_{,x}$ and $\phi_{,x}$ as local values along the beam, i.e., functions of x, according to the local values of the resultant torsional moment M_x and the axial force P.

Concluding Remarks

A study of the similarities between solid and thin-walled composite beams has been presented. For that purpose, a set of closed-form analytic solutions for solid and thin-walled composite beams were discussed. These solutions were examined by their adequacy to predict general characteristics of composite beams beyond the specific configuration and lamination modes that they were derived for. The study has been based on correlation with both available experimental data and calculated results of numerical schemes.

The findings of the present study clearly indicate that there are important similarities between the structural behavior and the composite-related structural mechanisms in composite beams that may be generalized by approximate analytic expressions. Specific examples are the twist–bending coupling mechanism in symmetric beams and the extension–torsion coupling in antisymmetric composite beams. It has been shown that the twist–bending coupling has been shown to be controlled by the same elastic moduli ratio for both solid and thin-walled beams. Similarly, the extension–torsion coupling in antisymmetric composite beams has been shown to be deter-

mined by the same elastic moduli ratio and cross-sectional geometric parameters in both solid and thin-walled beams.

Overall, it may be concluded that if interpreted correctly, the set of closed-form solutions that has been studied does supply a clear analytic insight into the coupling mechanisms for both solid and thin-walled composite beams. In addition, the generalization offered by the present study provides strength of materials-type expressions for preliminary estimation of the coupled structural behavior of generic composite beams. Nevertheless, there are cases where the similarities indicate correctly only the trend and the influential parameters but not the associated magnitude of the phenomenon. This may emerge from a lack of proper similarities in material property and ply-angle definitions, and it is recommended to continue study in this direction.

Appendix A: Reduced Stress-Strain Relations

The general constitutive relations for an unbalanced orthotropic lamina that is parallel to the x–y plane and the principal axis of which does not coincide with the x direction, may be written as

$$\{\boldsymbol{\sigma}\} = [C]\{\boldsymbol{\varepsilon}\} \tag{A1}$$

where the stiffness matrix $[C]$ is given by

$$[C] = \begin{bmatrix} C'_{11} & C'_{12} & C'_{13} & 0 & 0 & C'_{16} \\ C'_{12} & C'_{22} & C'_{23} & 0 & 0 & C'_{26} \\ C'_{13} & C'_{23} & C'_{33} & 0 & 0 & C'_{36} \\ 0 & 0 & 0 & C'_{44} & C'_{45} & 0 \\ 0 & 0 & 0 & C'_{45} & C'_{55} & 0 \\ C'_{16} & C'_{26} & C'_{36} & 0 & 0 & C'_{66} \end{bmatrix} \tag{A2}$$

The elastic moduli C'_{ij} are functions of the material properties and the ply angle relative to the x axis, e.g., Ref. 30, and $\{\boldsymbol{\sigma}\}$ and $\{\boldsymbol{\varepsilon}\}$ are the stress and strain vectors, respectively, namely,

$$\{\boldsymbol{\sigma}\} = \langle \sigma_{xx}, \sigma_{yy}, \sigma_{zz}, \tau_{yz}, \tau_{xz}, \tau_{xy} \rangle \tag{A3}$$

$$\{\boldsymbol{\varepsilon}\} = \langle \varepsilon_{xx}, \varepsilon_{yy}, \varepsilon_{zz}, \gamma_{yz}, \gamma_{xz}, \gamma_{xy} \rangle \tag{A4}$$

Assuming $\sigma_{yy} = \sigma_{zz} = \tau_{yz} = 0$ enables the expression ε_{yy}, ε_{zz}, and γ_{yz} in terms of ε_{xx}, γ_{xz}, and γ_{xy} as

$$\begin{Bmatrix} \boldsymbol{\varepsilon}_{yy} \\ \boldsymbol{\varepsilon}_{zz} \\ \boldsymbol{\gamma}_{yz} \end{Bmatrix} = \frac{1}{\Delta} \times \begin{bmatrix} C'_{23}C'_{13} - C'_{33}C'_{12} & 0 & C'_{23}C'_{36} - C'_{33}C'_{26} \\ C'_{23}C'_{12} - C'_{22}C'_{13} & 0 & C'_{23}C'_{26} - C'_{22}C'_{36} \\ 0 & -\dfrac{\Delta C'_{45}}{C'_{44}} & 0 \end{bmatrix} \begin{Bmatrix} \boldsymbol{\varepsilon}_{xx} \\ \boldsymbol{\gamma}_{xz} \\ \boldsymbol{\gamma}_{xy} \end{Bmatrix} \tag{A5}$$

where $\Delta = C'_{22}C'_{33} - C'^2_{23}$. By resubstituting Eq. (A5) in Eq. (A1), the reduced stress-strain relations of Eq. (3) are obtained where

$$C_{11} = C'_{11} - \frac{C'_{33}C'^2_{12} + C'_{22}C'^2_{13} - 2C'_{23}C'_{12}C'_{13}}{\Delta} \tag{A6a}$$

$$C_{16} = C'_{16} - \frac{C'_{12}(C'_{33}C'_{26} - C'_{23}C'_{36}) + C'_{13}(C'_{22}C'_{36} - C'_{23}C'_{26})}{\Delta} \tag{A6b}$$

$$C_{55} = C'_{55} - \frac{C'^2_{45}}{C'_{44}} \tag{A6c}$$

$$C_{66} = C'_{66} - \frac{C'_{33}C'^2_{26} + C'^2_{36} - 2C'_{23}C'_{26}C'_{36}}{\Delta} \tag{A6d}$$

References

[1]Bull, J. W. (ed.), "Numerical Analysis and Modelling of Composite Materials," *Analysis of Composite Rotor Blades*, Chapman & Hall, London, Dec. 1995, Chap. 1.

[2]Hong, C. H., and Chopra, I., "Aeroelastic Stability of a Composite Blade," *Journal of the American Helicopter Society*, Vol. 30, No. 2, 1985, pp. 57–67.

[3]Yuan, K., Friedmann, P. P., and Venkatesan, C., "Aeroelastic Behavior of Composite Rotor Blades with Swept Tips," *Proceedings of the American Helicopter Society 48th Annual Forum* (Washington, DC), American Helicopter Society, Alexandria, VA, 1992, pp. 1039–1059.

[4]Morison, W. D., "The Effect of Moisture Loss and Elevated Temperature upon the Material Damping of Fiber Reinforced Polymer Matrix Composites," Univ. of Toronto Inst. for Aerospace Studies (UTIAS), Rept. 324, Toronto, Canada, July 1988.

[5]Llanos, A. S., Lucchetto, L. A., Stafford, D., and Coulliette, C., "Environmental Conditions for Certification Testing of Helicopter Advanced Composite Main Rotor Components," 48th Annual Forum of the American Helicopter Society, Washington, DC, June 1992.

[6]Liu, S., Kutlu, Z., and Chang, F. K., "Matrix Cracking and Delamination in Laminated Composite Beams Subjected to a Transverse Concentrated Line Load," *Journal of Composite Materials*, Vol. 27, No. 5, 1993, pp. 436–470.

[7]Noor, A. K., and Burton, W. S., "Assessment of Shear Deformation Theories for Multilayered Composite Plates," *Applied Mechanics Reviews*, Vol. 42, No. 1, 1989, pp. 1–13.

[8]Gordaninejad, F., and Ghazavi, A., "Effect of Shear Deformation on Bending of Laminated Composite Beams," *Journal of Pressure Vessel Technology, Transactions of the ASME*, Vol. 111, No. 2, 1989, pp. 159–164.

[9]Nosier, A., and Reddy, J. N., "On Vibration and Buckling of Symmetric Laminated Plates According to Shear Deformation Theories," *Acta Mechanica*, Vol. 94, No. 3–4, 1992, pp. 123–169.

[10]Maiti, D. K., and Sinha, P. K., "Bending and Free Vibration Analysis of Shear Deformable Laminated Composite Beams by Finite Element Methods," *Journal of Composite Structures*, Vol. 29, No. 1, 1994, pp. 421–431.

[11]Zapfe, J. A., and Lesieutre, G. A., "Iterative Calculation of the Transverse Shear Distribution in Laminated Composite Beams," *Proceedings of the AIAA/ASME/ASCE/AHS/ASC 36th Structures, Structural Dynamics, and Materials Conference and AIAA/ASME Adaptive Structures Forum* (New Orleans, LA), AIAA, Washington, DC, 1995, pp. 3117–3125.

[12]Wang, S. S., and Choi, I., "Boundary-Layer Effects in Composite Laminates: Part 1—Free Edge Stress Singularities," *Journal of Applied Mechanics*, Vol. 49, No. 1, 1982, pp. 541–548.

[13]Wang, S. S., and Choi, I., "Boundary-Layer Effects in Composite Laminates: Part 2—Free Edge Stress Solutions and Basic Characteristics," *Journal of Applied Mechanics*, Vol. 49, No. 1, 1982, pp. 549–560.

[14]Rand, O., "Interlaminar Shear Stresses in Solid Composite Beams Using a Complete Shear Deformation Model," AIAA/ASME/ASCE/AHS/ASC 37th Structures, Structural Dynamics, and Materials Conf., Salt Lake City, UT, April 1996.

[15]Kosmatka, J. B., and Friedmann, P. P., "Structural Dynamic Modeling of Advanced Composite Propellers by the Finite Element Method," *Proceedings of the AIAA/ASME/ASCE/AHS 28th Structures, Structural Dynamics, and Materials Conference* (Monterey, CA), AIAA, Washington, DC, 1987, pp. 111–124.

[16]Kosmatka, J. B., and Friedmann, P. P., "Vibration Analysis of Composite Turbopropellers Using a Nonlinear Beam-Type Finite Element Approach," *AIAA Journal*, Vol. 27, No. 11, 1989, pp. 1606–1614.

[17]Stemple, A. D., and Lee, S. W., "A Finite Element Model for Composite Beams Undergoing Large Deflections with Arbitrary Cross Sectional Warping." *International Journal for Numerical Methods in Engineering*, Vol. 28, No. 9, 1989, pp. 2143–2163.

[18]Giavotto, V., Borri, M., Mantegazza, P., Ghiringhelli, G., Carmaschi, V., Maffioli, G. C., and Mussi, F., "Anisotropic Beam Theory and Applications," *Computers and Structures*, Vol. 16, Nos. 1–4, 1983, pp. 403–413.

[19]Perngjin, F. P., and Nayfeh, A. H., "A Fully Nonlinear Theory of Curved and Twisted Composite Rotor Blades Accounting for Warping and Three-Dimensional Stress Effects," *International Journal of Sol-*

ids and Structures, Vol. 31, No. 9, 1994, pp. 1309–1340.

[20]Fish, J. C., "Stress Analysis of Composite Rotor Systems," 47th Annual Forum of the American Helicopter Society, Phoenix, AZ, May 1991.

[21]Kalfon, J. P., and Rand, O., "Nonlinear Analysis of Composite Thin-Walled Helicopter Blades," *Journal of Computers and Structures*, Vol. 48, No. 1, 1993, pp. 51–61.

[22]Rand, O., "Nonlinear Analysis of Orthotropic Beams of Solid Cross-Sections," *Journal of Composite Structures*, Vol. 29, No. 1, 1994, pp. 27–45.

[23]Minguet, P., and Dugundji, J., "Experiments and Analysis for Composite Blades Under Large Deflections, Part I: Static Behavior," *AIAA Journal*, Vol. 28, No. 9, 1990, pp. 1573–1579.

[24]Minguet, P., and Dugundji, J., "Experiments and Analysis for Composite Blades Under Large Deflections, Part II: Dynamic Behavior," *AIAA Journal*, Vol. 28, No. 9, 1990, pp. 1580–1588.

[25]Chandra, R., Stemple, A. D., and Chopra, I., Thin-Walled Composite Beams Under Bending, Torsional, and Extensional Loads," *Journal of Aircraft*, Vol. 27, No. 7, 1990, pp. 619–626.

[26]Chandra, R., and Chopra, I., "Vibration Characteristics of Composite I-Beam with Elastic Couplings Under Rotation," 47th Annual Forum of the American Helicopter Society, Phoenix, AZ, May 1991.

[27]Berdichevsky, E. A., Armanios, E., and Ashraf, B., "Theory of Anisotropic Thin-Walled Closed-Cross-Section Beams," *Composite Engineering*, Vol. 2, Nos. 5–7, 1992, pp. 411–432.

[28]Rand, O., and Barkai, S. M., "Analytic Insight into the Structural Couplings and Nonlinear Formulation of Solid and Thin-Walled Composite Blades," American Helicopter Society 52nd Annual Forum, Washington, DC, June 1996.

[29]Timoshenko, S. P., and Goodier, J. N., *Theory of Elasticity*, 3rd ed., McGraw–Hill, New York, 1970.

[30]Ochoa, O. O., and Reddy, J. N., *Finite Element Analysis of Composite Laminates*, Kluwer, Dordrecht, The Netherlands, 1992.

[31]Sun, C. T., and Li, S., "Three-Dimensional Effective Elastic Constants for Thick Laminates," *Journal of Composite Materials*, Vol. 22, No. 7, 1988, pp. 629–639.

[32]Sokolnikoff, I. S., *Mathematical Theory of Elasticity*, 2nd ed., McGraw–Hill, New York, 1956.